

# Dynamic Analysis of Ferroelectric Negative Capacitance - Electrostatic MEMS Hybrid Actuators

Raghuram.T.R and Arvind Ajoy

**Abstract**—Electrostatic Micro-Electro Mechanical Systems (MEMS) actuators are a key element in today’s electronic switching applications. One of the main challenges in realizing a heterogeneous system having such MEMS actuators along with other CMOS devices is the high operating voltage of the MEMS actuator. In this work, we propose a SPICE based framework to model ferroelectric negative capacitance - electrostatic MEMS hybrid actuators. Using this framework, we demonstrate that the negative capacitance of the ferroelectric can result in a significant reduction in the dynamic pull-in and pull-out voltages of the actuator. We also show the effect of ferroelectric thickness on these voltages and the effect of ferroelectric damping on the energy dissipation. Our proposal shows that the hybrid actuator is better than the standalone MEMS actuator in terms of voltage requirement and energy dissipation. We also reveal the trade-off between the operating voltage and the pull-in time.

**Index Terms**—Ferroelectric negative capacitance, electrostatic MEMS actuator, dynamic pull-in, SPICE modeling.

## I. INTRODUCTION

**M**ICRO Electro Mechanical Systems (MEMS) based on electrostatic actuation and sensing are an integral part of today’s electronics. The ITRS roadmap describes the significance of many such devices in applications ranging from consumer - to - automotive - to - medical electronics [1]. Electrostatic MEMS actuators are very popular and are widely used because of their inherent low power consumption. The response of such electrostatic MEMS actuators to voltage excitation is different for static and dynamic [2]–[6] inputs. The former corresponds to the input voltage being varied slowly, so that the actuator is in quasi-static equilibrium. The latter corresponds to the input voltage being varied suddenly, as in the case of a step voltage excitation. Electrostatic actuators with step voltage excitation (dynamic) play a key role in switching (like RF MEMS switches) and display applications [7]–[11]. However, the operating voltages of such electrostatic MEMS actuators are typically much larger than the supply voltages used in modern CMOS integrated circuits. Realization of low-voltage electrostatic MEMS switches will enable a seamless integration of MEMS with CMOS electronics.

A novel technique to realize low-voltage electrostatic MEMS actuators was proposed and its static response was analyzed analytically in Ref. [12]. The idea was to connect a ferroelectric capacitor exhibiting negative capacitance in series with the MEMS actuator, thus forming a ferroelectric

Raghuram.T.R is with the Department of Electrical Engineering, Indian Institute of Technology Palakkad, Palakkad, India. e-mail: 121704004@smail.iitpkd.ac.in

Arvind Ajoy is with the Department of Electrical Engineering, Indian Institute of Technology Palakkad, Palakkad, India. e-mail: arvindajoy.iitpkd.ac.in

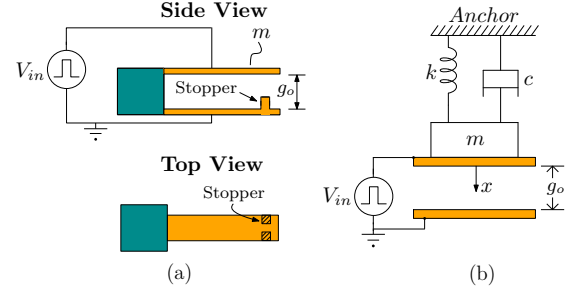


Fig. 1. An example of modeling a generic electrostatic MEMS actuator using a 1-DOF model. (a) Cantilever MEMS (b) Equivalent 1-DOF model capturing the essential features of the cantilever structure.

negative capacitance - electrostatic MEMS hybrid actuator. As described earlier, dynamic pull-in and pull-out analysis is however more relevant for switching applications than static analysis. To the best of our knowledge, dynamic pull-in and pull-out analysis of these hybrid actuators has not yet been reported.

In this work, we model the hybrid actuator numerically using SPICE and analyze its dynamic response. SPICE based modeling is circuit compatible and thus it can facilitate evaluation of circuit performance of various heterogeneous CMOS-MEMS systems easily. Using this approach, we demonstrate sub 1V dynamic operation of the hybrid actuator, enabling the integration of such MEMS actuators with modern CMOS devices. This eliminates the need of additional on-chip voltage sources and drive electronics used in present day MEMS-CMOS hybrid integrated circuits [13]–[16]. This also eliminates the scaling down of the structural parameters, such as air-gap  $g_0 < 10 \text{ nm}$ , of the MEMS actuator to achieve low-voltage operation [17]–[19]. With this model, the effect of ferroelectric thickness on the operating voltages is also illustrated. Further, the effect of ferroelectric damping and the pull-in time analysis are also presented.

This paper is organized as follows. Section II reviews the dynamics of a standalone electrostatic MEMS actuator. Section III presents the modeling of the ferroelectric negative capacitance - electrostatic MEMS hybrid actuator using SPICE. Simulation results and discussion are detailed in section IV. Section V presents our conclusion.

## II. REVIEW OF DYNAMICS OF ELECTROSTATIC MEMS ACTUATOR

In this work, we model a generic standalone electrostatic MEMS actuator as a single degree of freedom (1-DOF), parallel plate arrangement consisting of a pair of electrodes

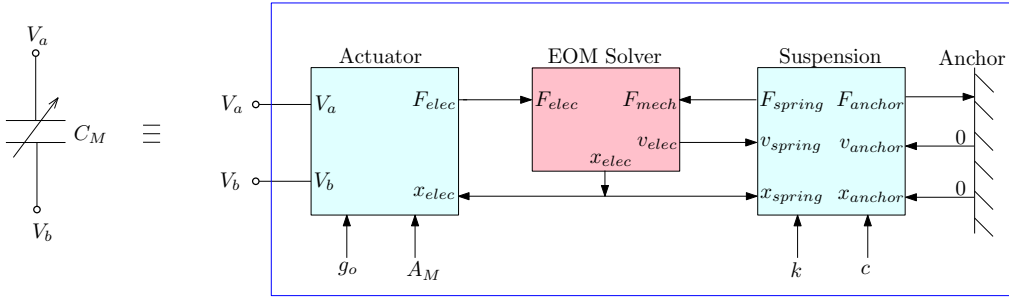


Fig. 2. SPICE model of standalone electrostatic MEMS actuator. Arrows pointing into (out of) a block refer to inputs (outputs) to (from) the block.  $x$  designates position,  $v$  designates velocity and  $F$  designates forces. Implementation of these blocks using circuit elements follows Ref. [20].

separated by an air-gap  $g_o$ . As shown in the Fig. 1, one electrode (bottom) is fixed and the other (top) is movable. The parameters used in the 1- DOF model (mass  $m$ , spring constant  $k$ , damping coefficient  $c$ ) represent their effective equivalents in the generic actuator. In this work, we set the damping coefficient to zero, so as to enable a comparison with analytical results wherever possible. For dynamic operation, a step voltage is applied to the actuator. Below a certain value of this applied step voltage, called the dynamic pull-in voltage, the response of the actuator is periodic. The maximum value of this periodic displacement of the electrode is called dynamic pull-in displacement. For applied step voltage above the dynamic pull-in voltage, the movable top electrode snaps down onto the bottom electrode. This condition is called dynamic pull-in [5]. After achieving pull-in, when the applied step voltage is decreased to a specific value, called the dynamic release voltage / pull-out voltage, the pull-in condition is lost and the movable electrode comes back to its original position. We assume that the MEMS actuator has a pair of stoppers, as shown in Fig. 1(a), to minimize the area of contact on pull-in and thus minimize the effect of surface forces. We hence neglect these forces in our analysis.

The equation of motion governing the actuator response to the applied voltage  $V_{in} u(t)$ , where  $u(t)$  is the unit step function, is given by

$$m \frac{d^2 x}{dt^2} + c \frac{dx}{dt} + k x = \frac{\epsilon_o A_M V_{in}^2}{2 (g_o - x)^2} \quad (1)$$

for  $t \geq 0$ .  $A_M$  is the area of the electrode,  $\epsilon_o$  is the permittivity of free space, and  $x$  is the dynamic variable representing the displacement of the electrode. With damping neglected, the dynamic pull-in voltage  $V_{PI}$  and the dynamic pull-in displacement  $X_{PI}$  are given by [11]

$$V_{PI} = \sqrt{\frac{k g_o^3}{4 \epsilon_o A_M}} \quad \text{and} \quad X_{PI} = \frac{g_o}{2} \quad (2)$$

Note that no analytical expression for dynamic release voltage has been reported in literature.

### III. MODELING FERROELECTRIC NEGATIVE CAPACITANCE - ELECTROSTATIC MEMS HYBRID ACTUATOR

The SPICE model of the standalone electrostatic MEMS is implemented as shown in Fig. 2. It consists of four modules namely the actuator, the suspension, the Equation of

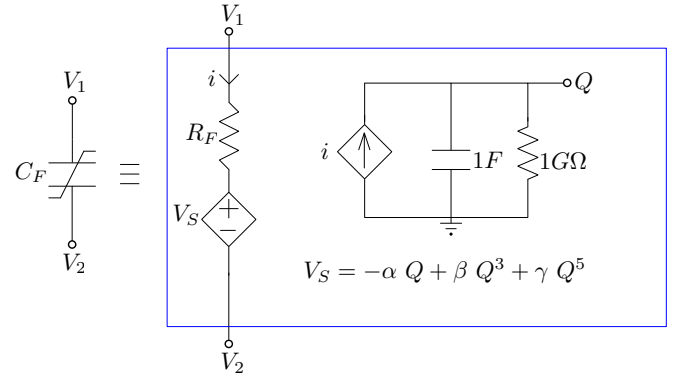


Fig. 3. SPICE model of ferroelectric capacitor. The charge  $Q$  is determined using an RC integrator. The voltage source  $V_S$  is implemented using arbitrary behavioral voltage source.

Motion (EOM) solver and the anchor [20]. These modules are represented as sub-circuits in the schematic along with their associated parameters as depicted in Fig. 2. The initial displacement and velocity of the movable electrode are taken as zero. The actuator module takes the applied step voltage  $V_{in}$ , area  $A_M$ , initial air-gap  $g_o$  and the electrode displacement  $x_{elec}$  as input parameters and calculates the electrostatic force  $F_{elec} = \epsilon_o A_M V_{in}^2 / 2 (g_o - x)^2$ . The suspension module takes the electrode displacement  $x_{elec}$ , electrode velocity  $v_{elec}$ , the spring constant  $k$  and the damping coefficient  $c$  as the input parameters and calculates the mechanical restoring force  $F_{mech} = c \cdot dx/dt + kx$ . The EOM solver module is placed between the actuator and suspension modules. The EOM solver compares the two forces  $F_{elec}$  and  $F_{mech}$  and calculates the resultant electrode displacement and velocity by solving Eq. (1) for the specified electrode mass  $m$ . Electrical feedback connection is provided within these blocks to reach the equilibrium solution of the electrode displacement numerically for the applied step voltage.

The dynamics of the ferroelectric capacitor (single domain) is captured by the time dependent Landau - Khalatnikov (LK) equation [21]–[26] relating the voltage  $V_F$  across the ferroelectric to charge  $Q$  as

$$V_F = -\alpha Q + \beta Q^3 + \gamma Q^5 + R_F \frac{dQ}{dt} \quad (3)$$

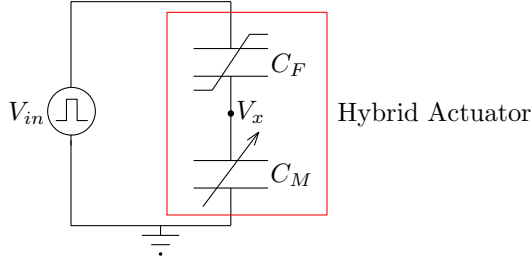


Fig. 4. Ferroelectric negative capacitance -electrostatic MEMS hybrid actuator equivalent circuit.  $C_F$  represents the ferroelectric capacitor and  $C_M$  represents the variable capacitance provided by the MEMS actuator.

$$\alpha = -\frac{\alpha_F t_F}{A_F}; \beta = \frac{\beta_F t_F}{A_F^3}; \gamma = \frac{\gamma_F t_F}{A_F^5}; R_F = \frac{\rho t_F}{A_F} \quad (4)$$

where  $\rho$  is the ferroelectric damping constant;  $\alpha_F$ ,  $\beta_F$  and  $\gamma_F$  are ferroelectric anisotropy coefficients,  $t_F$  is the thickness of the ferroelectric, and  $A_F$  is the area of the ferroelectric. The last term of Eq. (3) denotes the voltage drop across resistor  $R_F$  with  $dQ/dt$  representing the current  $i$  through it. Thus, Eq. (3) is implemented in SPICE as a Voltage Controlled Voltage Source (VCVS) in series with resistor  $R_F$ . The SPICE model of the ferroelectric capacitor is shown in Fig. 3. The charge  $Q$  is estimated by integrating the current  $i$  through the capacitor [27].

The ferroelectric negative capacitance - electrostatic MEMS hybrid actuator is modeled in SPICE by cascading a ferroelectric capacitor  $C_F$  with the standalone MEMS actuator (depicted as a variable capacitor  $C_M$ ) as shown in Fig. 4. The intermediate node voltage  $V_x$  is obtained as

$$V_x = V_{in} \frac{C_F}{C_F + C_M} \quad (5)$$

Since the ferroelectric capacitor offers negative capacitance, Eq. (5) can be rewritten as

$$V_x = V_{in} \frac{|C_F|}{|C_F| - C_M} \quad (6)$$

When the absolute value of ferroelectric capacitance  $|C_F|$  is close to the MEMS capacitance  $C_M$ , the intermediate node voltage shows voltage amplification. Thus the MEMS actuator requires a reduced voltage to achieve pull-in. This is the key principle behind reduction in the dynamic pull-in voltage of the electrostatic MEMS actuator in the presence of a series ferroelectric capacitor.

#### IV. SIMULATION RESULTS AND DISCUSSION

Table I lists the parameters of the hybrid actuator used in the simulation. SBT ( $\text{Sr}_{0.8}\text{Bi}_{2.2}\text{Ta}_2\text{O}_9$ ) is used as the ferroelectric material. The ferroelectric layer thickness and area are designed so as to obtain a static pull-in voltage of 0.8V and a static pull-out voltage of 0V, using the equations available in Ref. [12]. The validation of the SPICE model for static pull-in and pull-out analysis can be found in the Appendix. As mentioned earlier, the movement of the top electrode is limited by means of a stopper of height  $h_s$ .

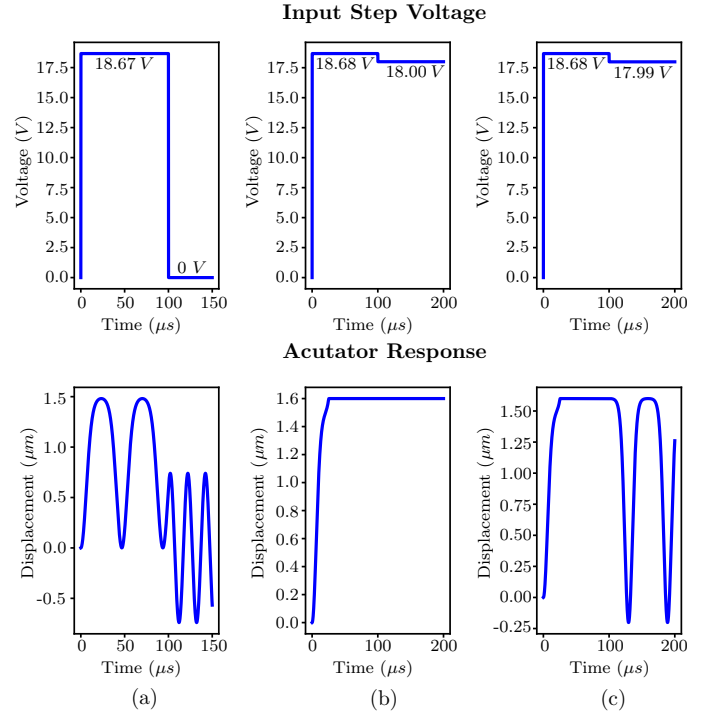


Fig. 5. Standalone electrostatic MEMS actuator dynamic response (a) Actuator response before dynamic pull-in showing a maximum displacement of  $1.5 \mu\text{m}$ . (b) Actuator response after dynamic pull-in and without release. (c) Actuator response after dynamic pull-in and with release.

Fig. 5 shows the simulated dynamic response of the standalone MEMS actuator. Eq. (2) predicts a dynamic pull-in voltage of 18.67 V and a pull-in displacement of  $1.5 \mu\text{m}$ . Our simulation results are consistent with these theoretical predictions. For input step voltage less than the dynamic pull-in voltage (18.67 V), the actuator response is periodic. For input step voltage greater than the dynamic pull-in voltage, the actuator achieves pull-in. A release voltage of 17.99 V is obtained from simulation.

The ferroelectric capacitor model is now connected in series

TABLE I  
FERROELECTRIC NEGATIVE CAPACITANCE - ELECTROSTATIC MEMS  
HYBRID ACTUATOR PARAMETERS FOR SPICE SIMULATION

Parameter	Value
Length of the cantilever, $L$	$160 \mu\text{m}$
Width of the cantilever, $W$	$6 \mu\text{m}$
Thickness of the cantilever, $T$	$2 \mu\text{m}$
Cantilever Material	Silicon (Si)
Young's Modulus, $E$	$150 \text{ GPa}$ [28]
Density, $D$	$2330 \text{ kg/m}^3$ [29]
Mass, $m$	$4.4736 \times 10^{-12} \text{ kg}$
Spring Constant, $k$	$0.439 \text{ N/m}$
Initial air-gap, $g_o$	$3 \mu\text{m}$
Stopper height, $h_s$	$1.4 \mu\text{m}$
Permittivity of free space, $\epsilon_o$	$8.854 \times 10^{-12} \text{ F/m}$
Ferroelectric Material	SBT ( $\text{Sr}_{0.8}\text{Bi}_{2.2}\text{Ta}_2\text{O}_9$ ) [12]
$\alpha_F$	$-6.5 \times 10^7 \text{ m/F}$
$\beta_F$	$3.75 \times 10^9 \text{ m}^5/\text{F}/\text{C}^2$
$\gamma_F$	$0 \text{ m}^9/\text{F}/\text{C}^4$
Ferroelectric Thickness, $t_F$	$5.99 \mu\text{m}$
Ferroelectric Area, $A_F$	$1.1659 \times 10^{-12} \text{ m}^2$

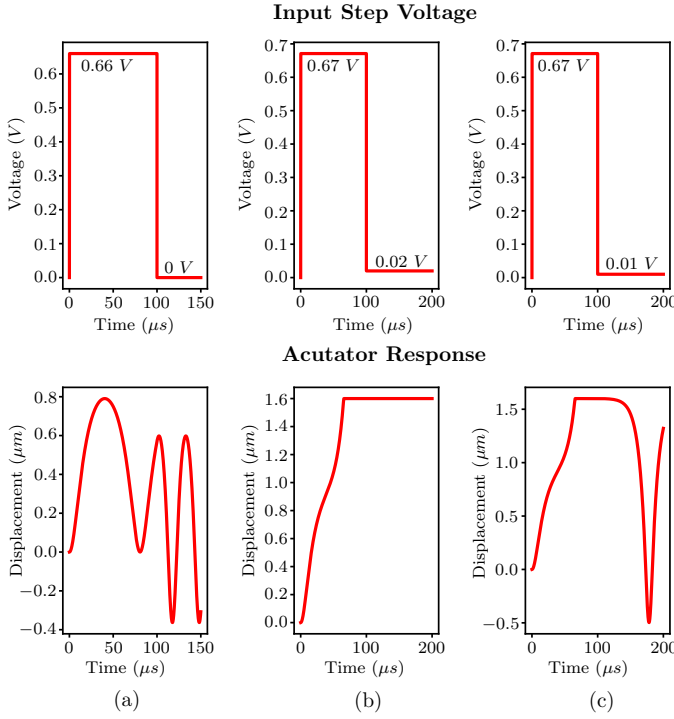


Fig. 6. Ferroelectric negative capacitance - electrostatic MEMS hybrid actuator dynamic response showing significant reduction in operating voltages. (a) Actuator response before dynamic pull-in. (b) Actuator response after dynamic pull-in and without release. (c) Actuator response after dynamic pull-in and with release.

to the standalone MEMS model to form the hybrid actuator. Again, the dynamic response of the hybrid actuator is obtained by applying a step input voltage as shown in Fig. 6. The dynamic pull-in and release voltages of the hybrid actuator are found to be  $0.66\text{ V}$  and  $0.01\text{ V}$  respectively. Compared to the standalone MEMS actuator, there is a significant reduction in the operating voltages of the hybrid actuator. This is because of the voltage amplification due to the negative capacitance of the series ferroelectric capacitor. This sub  $1\text{ V}$  operation of the hybrid actuator should allow seamless integration of such

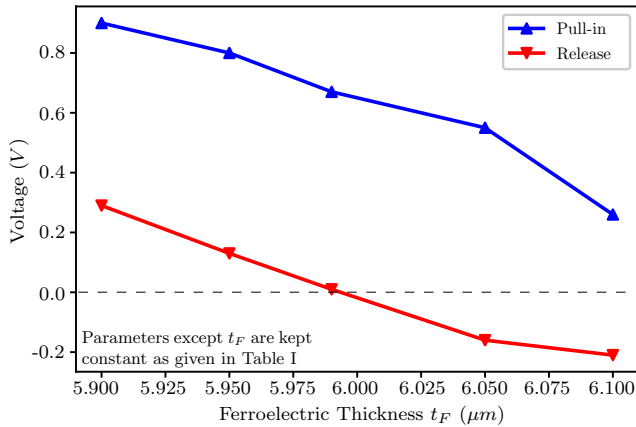


Fig. 7. Effect of ferroelectric thickness  $t_F$  on the dynamic pull-in and release voltages of the hybrid actuator depicting the possibility of obtaining both positive and negative release voltages by proper choice of ferroelectric thickness.

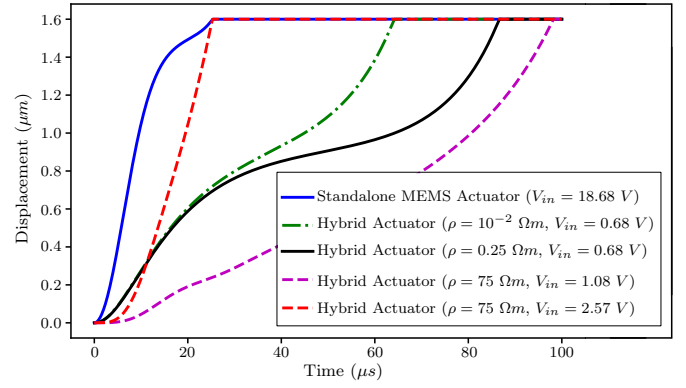


Fig. 8. Dynamic pull-in time analysis of standalone MEMS actuator and hybrid actuator. It is shown that the hybrid actuator is slower in comparison with the standalone MEMS actuator to achieve dynamic pull-in. There also exists a trade-off between the applied step voltage and the pull-in time.

MEMS actuators with modern CMOS devices, eliminating the need of any drive electronics or additional on-chip voltage up-converters.

The effect of ferroelectric thickness  $t_F$  on the dynamic pull-in and release voltages is shown in Fig. 7. Increase in the ferroelectric thickness reduces the operating voltages. This is because, with increase in ferroelectric thickness, the ferroelectric capacitance decreases leading to enhanced voltage amplification. This is in agreement with a similar trend observed in ferroelectric negative capacitance - FET devices [24] where the gate voltage reduces with increase in ferroelectric thickness. However, the ferroelectric thickness should be properly chosen (i.e.  $|C_F| \sim C_M$ ) so as to preserve the voltage amplification phenomenon. Note that the release voltage can be either positive or negative. Negative release voltage is favourable for bipolar voltage actuation of electrostatic MEMS actuators leading to improved reliability [30], [31] and also in memory applications [32]. However, this requires both positive and negative power supplies for operation. Tailoring ferroelectric thickness  $t_F$  can also ensure  $0\text{ V}$  release voltage facilitating the use of single sub  $1\text{ V}$  voltage source for both pull-in and

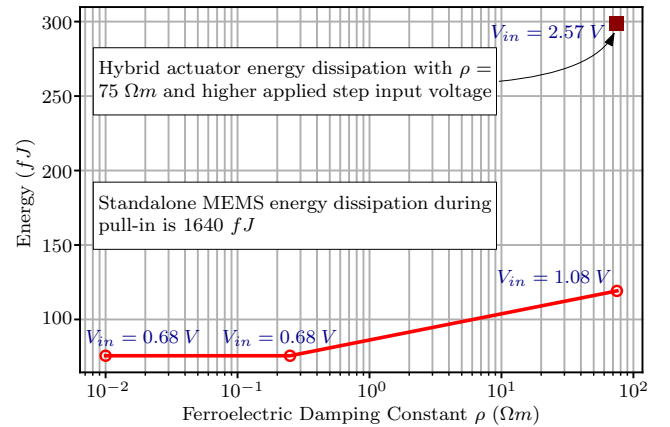


Fig. 9. Effect of ferroelectric damping constant  $\rho$  on the energy dissipation during dynamic pull-in in the hybrid actuator. Note that there is reduction in the energy dissipation in comparison with the standalone MEMS actuator due to reduction in the dynamic pull-in voltage.

release. For example, a hybrid actuator with  $t_F = 6.10 \mu m$  has a negative release voltage ( $-0.21 V$ ), which implies that a reduction of the applied voltage to  $0 V$  will not result in release. However, a small change in thickness to  $5.95 \mu m$  (with release voltage  $0.13 V$ ) will ensure release of the cantilever at  $0 V$ .

A temporal analysis of dynamic pull-in of the standalone MEMS actuator and the hybrid actuator is shown in Fig. 8. The release process is not considered as displacement by only few nanometers is sufficient to release the electrode. Ferroelectric damping, modeled by the resistance  $R_F = \rho t_F/A_F$  in the SPICE model of the ferroelectric capacitor, plays an important role in the time response of the hybrid actuator. A large range of  $\rho$  is used in the simulation for a comprehensive prognosis. Note that we have used the values of  $\rho$  reported in literature for PZT [23], [24] since we could not find the corresponding values for SBT. The pull-in voltage is a function of  $\rho$ . For each value of the ferroelectric damping constant, a step input voltage slightly greater than the pull-in voltage, is used for actuation. It is observed that the hybrid actuator is slower in comparison with the standalone MEMS actuator. However, note that there is a trade-off between the applied step input voltage and the pull-in time – a larger step input voltage will result in faster pull-in of the actuator. This suggests that, by applying a higher step voltage (which is still smaller than that of the standalone actuator), the pull-in time of the hybrid actuator can be made equal to the pull-in time of the standalone actuator. This ensures low-voltage operation of the hybrid actuator without compromising on the pull-in time. For example, both standalone MEMS actuator and hybrid actuator with  $\rho = 75 \Omega m$  and step input voltage  $V_{in} = 2.57 V$  have the same dynamic pull-in time as depicted in Fig. 8.

Electrostatic MEMS actuators are inherently low-power devices owing to their near zero power dissipation [33], [34]. Reduction in the operating voltages further can potentially reduce the power dissipation during switching and thus enabling the use of such actuators in low-power, low-voltage applications. We estimate the energy for pull-in as time integral of the instantaneous power  $v(t) \cdot i(t)$  over the entire pull-in time. Fig. 9 shows the results of the above calculation. Again, ferroelectric damping constant  $\rho$  plays an important role. As in the case of temporal analysis, we apply a step voltage of value slightly larger than the pull-in voltage in each case to ensure pull-in. Note that the energy dissipated during pull-in in the standalone MEMS actuator is  $1640 fJ$ . The energy dissipated during pull-in in the hybrid actuator for different values of  $\rho$  varies between  $50$ - $150 fJ$ . For example, for  $\rho = 75 \Omega m$ , the energy dissipated during pull-in is  $119.17 fJ$ . This shows a  $10x$  reduction in the energy dissipation using the hybrid actuator. However, this reduction in energy comes at the cost of slower pull-in. In the previous paragraph, we showed that the actuator can be operated using a voltage higher than pull-in voltage to achieve a pull-in time identical to that of the standalone MEMS actuator. Fig. 9 also shows the energy dissipated when the hybrid actuator with  $\rho = 75 \Omega m$  is actuated with a step voltage  $V_{in} = 2.57 V$ . We find that the energy dissipated is still  $5x$  lower than the energy dissipated in the standalone actuator, indicating a very

favourable application of the trade-off between pull-in time and applied voltage.

## V. CONCLUSION

The dynamic analysis of ferroelectric negative capacitance - electrostatic MEMS hybrid actuators based on SPICE multi-physics model is presented in this work. It is shown that the dynamic pull-in and release voltages of this hybrid actuator are significantly reduced due to the presence of the series ferroelectric capacitor. This allows straightforward integration of such actuators with modern CMOS devices. Further, this also opens the door for the use of such actuators in low-power, low-voltage applications. The effect of ferroelectric thickness in achieving both positive and negative release voltage is also illustrated. There is considerable reduction in the energy dissipated in the hybrid actuator in comparison with the standalone MEMS actuator, accompanied by an increase in pull-in time, when the actuator is actuated with a voltage slightly above the pull-in voltage. However, we can trade-off pull-in time versus applied voltage to achieve identical pull-in times for the hybrid and standalone actuators and still achieve reduction in the energy dissipated in hybrid actuator. Finally, since the model is SPICE based and thus circuit compatible, this can be used in conjunction with other low-voltage CMOS circuits to realize various heterogeneous CMOS - MEMS systems.

## APPENDIX

The static pull-in voltage  $V_{SPI}$  and the travel range  $X_{Tr}$  of the hybrid actuator is given by

$$V_{SPI} = r_{\alpha N} \sqrt{\frac{r_{\alpha N}}{r_{\beta N}} \cdot \frac{8 k g_o^3}{27 \epsilon_0 A_M}}; X_{Tr} = \frac{r_{\alpha N}}{r_{\beta N}} \cdot \frac{g_o}{3} \quad (A1)$$

where

$$r_{\alpha N} = 1 - \frac{t_F A_M |\alpha_F| \epsilon_o}{g_o A_F} \quad (A2)$$

$$r_{\beta N} = 1 - \left[ (2 \beta_F k \epsilon_o^2) \left( \frac{t_F A_M^2}{A_F^3} \right) \right] \quad (A3)$$

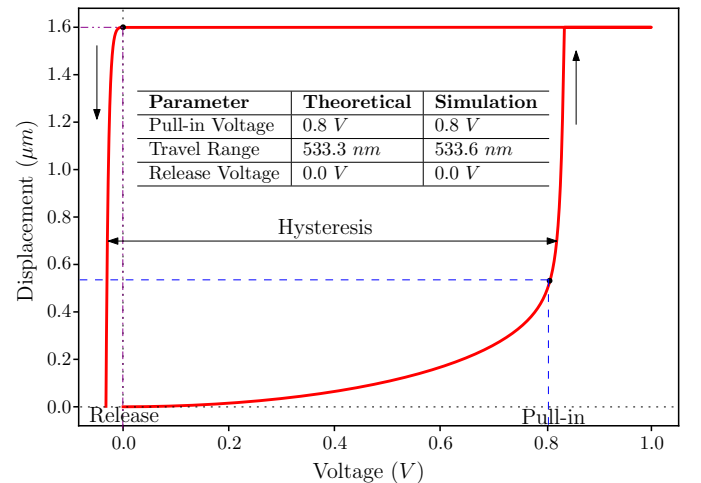


Fig. A1. Static pull-in and release characteristics of the hybrid actuator. The simulation results are in agreement with the analytical results given in Ref. [12], thus validating the hybrid actuator SPICE model.

Assuming zero static release voltage, we have  $g_o - h_s = (r_{\alpha N}/r_{\beta N}) g_o$ . Thickness  $t_F$  and area  $A_F$  are designed so as to obtain  $V_{SPI} = 0.8 V$ . The static pull-in and release characteristics of the hybrid actuator is shown in Fig. A1. From the simulation, the static pull-in voltage is obtained as that particular voltage when the displacement equals the travel range. The simulation results are in agreement with the analytical results given in Ref. [12], thus validating the hybrid actuator SPICE model.

#### ACKNOWLEDGEMENT

The authors thank Dr. Revathy Padmanabhan and Dr. Sukomal Day, Indian Institute of Technology Palakkad for helpful discussions.

#### REFERENCES

- [1] "2015 International Technology Roadmap for Semiconductors (ITRS)," Tech. Rep., Jun. 2015.
- [2] M. I. Younis, *MEMS Linear and Nonlinear Statics and Dynamics*. Boston, MA: Springer US, 2011, vol. 20, doi:10.1007/978-1-4419-6020-7.
- [3] L. A. Rocha, E. Cretu, and R. F. Wolffenbuttel, "Pull-in dynamics: Analysis and modeling of the transitional regime," in *Proc. 17th IEEE Int. Conf. MEMS*, Jan. 2004, pp. 249–252, doi:10.1109/MEMS.2004.1290569.
- [4] D. Elata, "On the static and dynamic response of electrostatic actuators," *Bull. Polish Acad. Sci.*, vol. 53, no. 4, pp. 373–384, Dec. 2005.
- [5] V. Leus and D. Elata, "On the dynamic response of electrostatic MEMS switches," *J. Microelectromech. Syst.*, vol. 17, no. 1, pp. 236–243, Feb. 2008, doi:10.1109/JMEMS.2007.908752.
- [6] W.-M. Zhang, H. Yan, Z.-K. Peng, and G. Meng, "Electrostatic pull-in instability in MEMS/NEMS: A review," *Sensors and Actuators A Physical*, vol. 214, pp. 187–218, Aug. 2014, doi:10.1016/j.sna.2014.04.025.
- [7] G. N. Nielson and G. Barbastathis, "Dynamic pull-in of parallel-plate and torsional electrostatic MEMS actuators," *J. Microelectromech. Syst.*, vol. 15, no. 4, pp. 811–821, Aug. 2006, doi:10.1109/JMEMS.2006.879121.
- [8] G. N. Nielson, R. H. Olsson, G. R. Bogart, P. R. Resnick, O. B. Spahn, C. Tigges, G. Grossetete, and G. Barbastathis, "Dynamic pull-in and switching for sub-pull-in voltage electrostatic actuation," in *Proc. 14th Int. Conf. Solid-State Sens., Actuators, Microsyst. (TRANSDUCERS)*, Jun. 2007, pp. 455–459, doi:10.1109/SENSOR.2007.4300166.
- [9] S. Shekhar, K. J. Vinoy, and G. K. Ananthasuresh, "Switching and release time analysis of electrostatically actuated capacitive RF MEMS switches," *Sens. Transducers*, vol. 130, no. 7, pp. 77–90, Jul. 2011.
- [10] G. M. Rebeiz, *RF MEMS: Theory, Design, and Technology*. John Wiley & Sons, 2004.
- [11] K. B. Lee, *Principles of Microelectromechanical Systems*. John Wiley & Sons, 2011.
- [12] M. Masuduzzaman and M. A. Alam, "Effective nanometer airgap of NEMS devices using negative capacitance of ferroelectric materials," *Nano Lett.*, vol. 14, no. 6, pp. 3160–3165, May. 2014, doi:10.1021/nl5004416.
- [13] G. M. Rebeiz, "RF MEMS switches: Status of the technology," in *Proc. 12th Int. Conf. Solid-State Sens., Actuators, Microsyst. (TRANSDUCERS)*, vol. 2, Jun. 2003, pp. 1726–1729, doi: 10.1109/SENSOR.2003.1217118.
- [14] N. Dumas, L. Latorre, F. Maily, and P. Nouet, "Design of a smart CMOS high-voltage driver for electrostatic MEMS switches," in *Symp. Design Test Integration and Packag. of MEMS/MOEMS (DTIP)*, May 2010, pp. 44–47.
- [15] J. F. Saheb, J. F. Richard, M. Sawan, R. Meingan, and Y. Savaria, "System integration of high voltage electrostatic MEMS actuators," *Analog Integr. Circ. Sig. Process.*, vol. 53, no. 1, pp. 27–34, Oct. 2007, doi:10.1007/s10470-006-9020-x.
- [16] J. A. Brandt, "High voltage bias waveform generator for an RF MEMS microswitch," Master's thesis, University of New Hampshire, Durham, 2008.
- [17] J. O. Lee, Y.-H. Song, M.-W. Kim, M.-H. Kang, J.-S. Oh, H.-H. Yang, and J.-B. Yoon, "A sub-1-volt nanoelectromechanical switching device," *Nature Nanotech.*, vol. 8, no. 1, pp. 36–40, Jan. 2013, doi:10.1038/nano.2012.208.
- [18] W. W. Jang, J. O. Lee, J.-B. Yoon, M.-S. Kim, J.-M. Lee, S.-M. Kim, K.-H. Cho, D.-W. Kim, D. Park, and W.-S. Lee, "Fabrication and characterization of a nanoelectromechanical switch with 15-nm-thick suspension air gap," *Appl. Phys. Lett.*, vol. 92, no. 10, p. 103110, Mar. 2008, doi:10.1063/1.2892659.
- [19] A. Attaran and R. Rashidzadeh, "Ultra low actuation voltage RF MEMS switch," *Micro and Nano Syst. Lett.*, vol. 3, no. 1, pp. 1–4, Dec. 2015, doi:10.1186/s40486-015-0024-0.
- [20] H. Toshiyoshi, "A SPICE-based multi-physics simulation technique for integrated MEMS," in *IEEE Int. Conf. Simulation of Semiconductor Processes and Devices*, Sep. 2011, pp. 239–242, doi: 10.1109/SISPAD.2011.6035069.
- [21] S. Salahuddin and S. Datta, "Use of negative capacitance to provide voltage amplification for low power nanoscale devices," *Nano Lett.*, vol. 8, no. 2, pp. 405–410, Feb. 2008, doi:10.1021/nl071804g.
- [22] A. I. Khan, K. Chatterjee, B. Wang, S. Drapcho, L. You, C. Serrao, S. R. Bakaul, R. Ramesh, and S. Salahuddin, "Negative capacitance in a ferroelectric capacitor," *Nature Mater.*, vol. 14, no. 2, pp. 182–186, Feb. 2015, doi:10.1038/nmat4148.
- [23] A. Aziz, S. Ghosh, S. Datta, and S. K. Gupta, "Physics-based circuit-compatible SPICE model for ferroelectric transistors," *IEEE Electron Device Lett.*, vol. 37, no. 6, pp. 805–808, Jun. 2016, doi:10.1109/LED.2016.2558149.
- [24] Y. Li, K. Yao, and G. S. Samudra, "Delay and power evaluation of negative capacitance ferroelectric MOSFET based on SPICE model," *IEEE Trans. Electron Devices*, vol. 64, no. 5, pp. 2403–2408, May. 2017, doi:10.1109/TED.2017.2674020.
- [25] Y. Li, Y. Kang, and X. Gong, "Evaluation of negative capacitance ferroelectric MOSFET for analog circuit applications," *IEEE Trans. Electron Devices*, vol. 64, no. 10, pp. 4317–4321, Oct. 2017, doi:10.1109/TED.2017.2734279.
- [26] A. I. Khan, "Negative capacitance for ultra-low power computing," Ph.D. dissertation, UC Berkeley, 2015.
- [27] M. Pešić, C. Küneth, M. Hoffmann, H. Mulaosmanovic, S. Müller, E. T. Breyer, U. Schroeder, A. Kersch, T. Mikolajick, and S. Slesazek, "A computational study of hafnia-based ferroelectric memories: from ab initio via physical modeling to circuit models of ferroelectric device," *J. Comput. Electron.*, vol. 16, no. 4, pp. 1236–1256, Dec. 2017, doi:10.1007/s10825-017-1053-0.
- [28] J. Kim, D. D. Cho, and R. S. Muller, "Why is (111) silicon a better mechanical material for MEMS?" in *Transducers 01 Eurosensors XV*. Springer, 2001, pp. 662–665, doi:10.1007/978-3-642-59497-7\_157.
- [29] J. F. Shackelford, Y.-H. Han, S. Kim, and S.-H. Kwon, *CRC Materials Science and Engineering Handbook*. CRC press, 2016.
- [30] Z. Peng, X. Yuan, J. C. Hwang, D. I. Forehand, and C. L. Goldsmith, "Dielectric charging of RF MEMS capacitive switches under bipolar control-voltage waveforms," in *Proc. IEEE/MTT-S Int. Microw. Symp.*, Jun. 2007, pp. 1817–1820, doi:10.1109/MWSYM.2007.380102.
- [31] M. Domínguez, D. López, D. Molinero, and J. Pons-Nin, "Dielectric charging control for electrostatic MEMS switches," in *Proc. SPIE*, vol. 7679, May 2010, pp. 1–11, doi:10.1117/12.853177.
- [32] W. Y. Choi, T. Osabe, and T.-J. K. Liu, "Nano-Electro-Mechanical nonvolatile memory (NEMory) cell design and scaling," *IEEE Trans. Electron Devices*, vol. 55, no. 12, pp. 3482–3488, Dec. 2008, doi:10.1109/TED.2008.2006540.
- [33] E. R. Brown, "RF-MEMS switches for reconfigurable integrated circuits," *IEEE Trans. Microw. Theory Tech.*, vol. 46, no. 11, pp. 1868–1880, Nov. 1998, doi:10.1109/22.734501.
- [34] G. M. Rebeiz and J. B. Muldavin, "RF MEMS switches and switch circuits," *IEEE Microw. Mag.*, vol. 2, no. 4, pp. 59–71, Dec. 2001, doi:10.1109/6668.969936.